WALL PRESSURE AND CONDITIONAL FLOW STRUCTURES IN THE REATTACHMENT REGION OF THE FLOW OVER A THICK PLATE

C. Sicot, R. Perrin, T. T. Tran, J. Borée
Institut Pprime, UPR CNRS 3346, ENSMA, Université de Poitiers,
BP 40109, 86961 Futuroscope Chasseneuil Cedex, France
(* corresponding author: christophe.sicot@ensma.fr)

ABSTRACT

The separating and reattaching flow over a thick plate with sharp angle at $Re = 80000$ is investigated using pressure and HS-PIV measurements. After having studied the mean flow properties, which are found in good agreement with the litterature, a particular emphasis is given concerning the eduction and the analysis of the evolution of the large scale vortices downstream of the reattachment. This is done using an adapted multi-time and multi-channel stochastic estimation of the velocity correlated with the wall pressure. Swirling strength and Finite Time Lyapunov Exponents are then used in order to detect and characterize the structures and their dynamics. Conditional statistics based on the feature longitudinal position are then computed in order to educe intensities, size, position and convection velocity of each conditional feature.

INTRODUCTION

Understanding the intrinsic spatial and unsteady features of separating and reattaching flows has a great importance for the design and control of a large amount of engineering applications. In particular, identification and tracking of critical points, such as vortices and saddle points, remains an important issue when dealing with unsteady flows. As part of a French ANR project (DIB: Dynamic, Unsteadiness, Noise), the present study investigates the turbulent flow generated by a blunt flat plate with right-angled corners at Reynolds number 80000. According to the literature (e.g. Kiya & Sasaki (1985)), large scale vortices shed from the shear layer are advected downstream of the mean reattachment point and dissipated into the outer boundary layer, as schematically described in figure 1. The objective here is twofold: to analyse the relationship between the shed structures and the wall fluctuating pressure, and to characterize their evolution downstream of the reattachment. To this aim, simultaneous High Speed PIV (HS-PIV) and wall pressure measurements have been carried out in the reattachment region. After having studied the mean flow properties, the fluctuating velocity correlated with the wall pressure is estimated using an adaptation of stochastic estimation, and the coherent structures are analysed using both Eulerian and Lagrangian criteria. The first section presents the experiment and the post-processing tools that have been developped. Following sections deals with the analysis of the mean motion, the eduction of the coherent vortices, and the evolution of these large scale vortices.

EXPERIMENTAL SET-UP and POST-PROCESSING

Flow Configuration

The experiments are performed in a 1/2 open throat anechoic low-speed Eiffel type's wind tunnel. The square nozzle section has dimensions of 460 mm $\times$ 460 mm. The blunt flat plate is e =30 mm thick, 1300 mm long and 460 mm wide giving a solid blockage of 6.5% and an aspect ratio of 15.3. The plate is parallel to the nominally smooth stream (fig. 1).

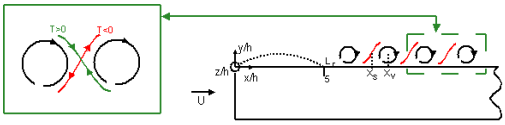

Figure 1. Schematic of the flow configuration and the ridge line of the FTLE field

The leading edge is located 300 mm downstream the jet outlet. The trailing edge is streamlined to minimize any wake-induced unsteadiness. The experiments are performed at a free-stream velocity U_0 =40 m.s^{-1} (Re=8.10^4 based on the thickness of the plate). The flow will be described henceforth using a cartesian co-ordinate system (x,y) to indicate the axial and vertical directions. The origin is set on the leading edge of the plate at the mean stagnation point. The corresponding velocity component are denoted by U and V. In the next sections, all the quantities are made non-dimensional using U_0 and e.

Measurements

HS-PIV HS-PIV systems have been used to record images of particles having a mean diameter of 1 μm. Illumination is provided by a New Wave PEGASUS Laser emitting two pulses of 10mJ (laser sheet thickness $\leq 1mm$). About 16 000 velocity fields were acquired with a PHOTRON ABX-RS camera in the symmetry plane y=0 at a frequency rate of 2kHz in order to obtain a long time interval of high speed PIV data.

The resolution of the sensor is 1024×1024 pixels^2 with a pixel size of 0.108mm/pixel. The time interval between two laser shots is fixed at 20 μm. A multipass algorithm with a final interrogation window size of 16×16 pixels^2 and 50% overlapping is applied. Spurious velocities are identified and replaced using both peak ratio and median filters. The maximum uncertainty on instantaneous velocity measurements are estimated at 0.54m/s (displacement of 0.1pixel). The TRPIV domain is located from $x/e \simeq 3$ to $x/e \simeq 10$. Other low frequency PIV plane upstream of the reattachment location have been acquired to complement the mean flow analysis.

Fluctuating pressure measurement The measurements of the surface fluctuating pressure are obtained with ten off-set sensors located from $x/e = 5.25$ to 8.6 downstream of the reattachment. Off-set sensors have the advantage to increase the pressure range of sensors because the fluctuating pressure decreases along the flexible tube between the pressure tab and the sensor. Those sensors are differential with a bandwidth of [0Hz-1.6kHz] and a pressure range of 250Pa. Details of the methodology are provided in Ruiz *et al.* (2010). The maximal error on fluctuating pressure is evaluated 9.4Pa. The sampling frequency is 5.12 kHz and a cut-off frequency of the anti-aliasing filters is set at 2 kHz. A square signal triggered by the Q-switch of the first laser cavity is used for the synchronisation of PIV and pressure aquisition.

Post-processing techniques

Stochastic estimation of the velocity field from the pressure data As will be seen in the the following section and in agreement with the litterature, a strong spatio-temporal coherence is found in a frequency range around $\frac{fe}{U_0} \simeq 0.12$, both in the velocity and in the pressure data. This coherence is to be related to the large scale vortices emanating from the separated shear layer and dissipating once embedded in the outer layer downstream of the reattachment. In order to analyse the spatio-temporal characteristics of these structures and their evolution, a multichannel and multitime version of stochastic estimation of the fluctuating velocity conditionned to the pressure traces has been developped. For comparison, classical LSE (Linear Stochastic estimation) have also been carried out. The classical LSE consists in finding the best approximation of the conditional velocity given p at the sensors location under the form $\tilde{u_i}(x,t) = B_j p_j(t)$ where p_j denotes the pressure at sensor j. Here the ten sensors described above are used for the estimation. The coefficients B_j are classically determined by solving the linear system $\overline{u_i p_k} = B_j \overline{p_j p_k}$ (Adrian (1979)). Two modifications are made to enhance the estimation: First, the pressure of the ten sensors are considered in a temporal window centred around the instant of the estimation. Second, a POD is performed on this spatio-temporal pressure data set (this technique is actually well-known as Multi-Channel Singular Spectrum Analysis in the meteorology field). The modes are then extended following the Extended POD procedure introduced by Borée (2003) to estimate the velocity fluctuations correlated with the pressure. This consist in taking the N first POD coefficients as the conditionning events in LSE and if all modes are considered, a multi-time LSE is recovered. This spatio-temporal technique was proposed by Perrin *et al.* (2008) to extract coherent patterns in the near wake of a cylinder and Ruiz *et al.* (2010) have then successfully applied the same technique in the wake of a disk above a flat plate. Two parameters has to be chosen in the procedure: the time window length T and the number of extended modes considered for the estimation. It is noticeable that keeping all modes and increasing T is actually a dangerous practice if the same data set is used for the determination of the extended modes and for the estimation (in this case, the term reconstruction is more appropriate) because 100% of the fluctuating energy can artifitially be reconstructued due to the finite data set available and a lack of convergence. Performing a prediction of a different data set with the same modes then results essentially in noise. Tests have been carried out by considering two subsets of the data, one used for the determination of the extended modes, the other to evaluate the quadratic error between the estimated and the original field. Different T and N were tested and an optimum has been found for a time window of approximately 2 shedding periods, and using $N = 40$ modes. The extended mode procedure presents two advantages over LSE: first, as just explained, it prevents from an artificially good estimation of the velocity due to a lack of convergence; second, the spatio-temporal POD filtering allows to filter out the small scale random contribution to the fluctuating pressure before performing the estimation. Altougth not shown in the paper due to space limitation, it is noticeable that the POD coefficients kept for the estimation have a spectral content in the same frequency range than the large scale vortical structures.

Finite Time Lyapunov Exponents The following short presentation of the FTLE theory is adapted from Garth *et al.* (2007). In a finite spatial and temporal domain, the position x of a fluid particle starting at a position x_0 at time $t = t_0$ is obtained by integration of the velocity field along the particle path. $x(t;t_0,x_0)$ satisfies $x(t_0;t_0,x_0) = x_0$ and $\dot{x}(t_0;t_0,x_0) = v(t,x)$, where the dot denotes the derivative with respect to the first parameter. By integrating all trajectories in the neighborhood of x_0 during the time T and after linearization, Haller (2001) showed that the maximum dispersion occurs in the unit direction associated with the largest eigenvalue λ_{max} of A^TA, where $A = \nabla_{x0}x(t_0+T;t_0,x_0)$ is the spatial gradient of the flow map after the integration time T. A^TA is the (right) finite time Cauchy-Green deformation tensor. To characterize an average exponential separation rate, the FTLE ${}^T_{t_0}\sigma(x_0)$ is then defined by ${}^T_{t_0}\sigma(x_0) = \frac{1}{T}.ln(\sqrt{\lambda_{max}})$. The calculation of the FTLE field (the integration can be done for positive and negative time, but here only negative time have been computed) then provides ridges which have to be regions associated with the presence of saddle point arising between two consecutive vortices (figure 1).

PIV data are not accurate close to the walls because of the reflection of the laser light (even though a special paint was used here). Therefore, a virtual PIV grid is extended down to and immediately under the wall. The velocity in this region is constructed by assuming that the wall is a slip boundary and a mirror instantaneous near wall flow is used to compute the trajectories. This approximation is valid because the viscous near wall length scales are small when compared to the coherent events (scaling with the thickness of the plate).

The instantaneous particle velocity at any time t is obtained by a spline interpolation of the spatiotemporal PIV ma-

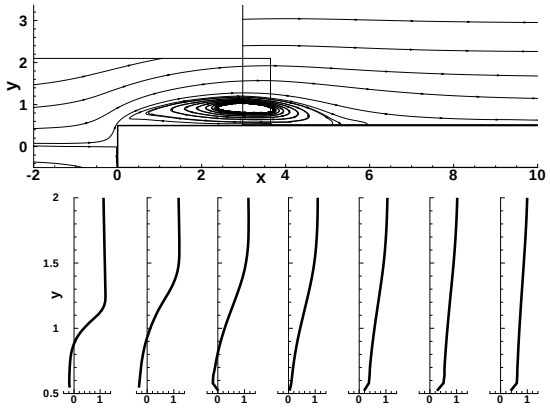

Figure 2. Streamlines of the mean flow (top) and ongitudinal mean velocity profiles at x/Xr=0.25, 0.5, 0.75, 1, 1.25, 1.5 and 1.75 (bottom)

trix. This three-dimensional matrix contains the temporal evolution of the planar velocity fields. For each instantaneous velocity field, the value of the FTLE at the center x_0 of a PIV interrogation window is computed by integrating the trajectories of its four neighbors during a time interval T. The spatial gradient $A = \nabla_{x0} x(t_0 + T; t_0, x_0)$ is then calculated using central differencing. A fourth-order Runge-Kutta method (RK4) is used to integrate the trajectories. After systematic tests and computations of trajectories, the time step dt used for RK4 computation was chosen equal to 0.1 ms. Finally, the value of the integration time T has to be chosen. A lower bound for T is technical and due to the repetition rate of the laser (2 kHz). This lower bound is $T_{min} = 1ms$ because it uses three consecutive velocity fields for the integration of a trajectory. The upper bound associated with this test is due to the fact that PIV data are only known over a finite domain. We are indeed unable to compute the flow map $x(t_0 - T; t_0, x_0)$ if T is too large. In fact, systematic tests showed that T=-2.5 ms is appropriate because the flow map is always computed in the domain of interest and the FTLE ridges are clearly defined.

Feature detection Two distincts features are detected in the estimated fields:

First, vortices are recognised as connex regions of swirling strength values λ_{ci} (Zhou *et al.* (1999)). For each region, the barycenter of λ_{ci} is used as a definition for the position (x_v, y_v) of the vortex. Area, maximum value of λ_{ci}, and the integral of λ_{ci} on the region, are also collected for each vortex. Tracking of these vortices is then performed in a rather simple way. Starting from a vortex at a given time step, the nearest vortex from an estimated position (using an estimation of a convection velocity) at the next time step, is considered to be the same vortex displaced during the time interval. A path is then deduced for each vortices during its passage in the PIV field, and an instantaneous convection velocity is determined by derivating of the path. Statistics are then calculated as functions of the longitudinal position x.

Second, the instantaneous locations of the saddle points, x_s, are then obtained by finding the positions of the FTLE local maximum on the instantaneous FTLE field. These local maximum are obtained with a spatial resolution of 1.73 mm because PIV fields are computed with a 50% overlap of the interrogation windows. The instantaneous saddle points detected have then been tracked in time with the same algorithm as that used to track the barycenters of the structures educed by swirling strength.

RESULTS AND ANALYSIS

Mean flow properties and spectra analysis

Streamlines of mean velocity field in the mid-span plane shows a reattachment length close to $X_r/e = 5.5$ (fig.2(top)). This reattachment length is in good agreement with results from literature where X_r is distributed over $[4, 5.5]$ for high Reynolds number flows (e.g. Kiya & Sasaki (1983)).

Profiles of the longitudinal time-mean velocity, U, are shown in figure 2(bottom).The maximum of reverse flow (about 0.3) is found at $x/X_r = 0.5$ i.e. at the centre of the separation bubble. A position where the vertical distribution of U has a point of inflexion can be interpreted as the centre of the shear layer. Figure 2 shows that this position is increasing for $x/X_r \leq 0.75$ whereas it changes slighthly for $x/X_r \geq 0.75$ where it is equal approximately to $y/e = 0.8$.

Figure 3 shows that the maximum of Reynolds stresses is found just upstream the reatteachment at a vertical position corresponding approximately to the heigth of the average separation bubble. At this position, maximum values of $\overline{u^2}$, $\overline{v^2}$ and $\overline{uv}$ are roughly 0.1, 0.05 and -0.04 respectively.

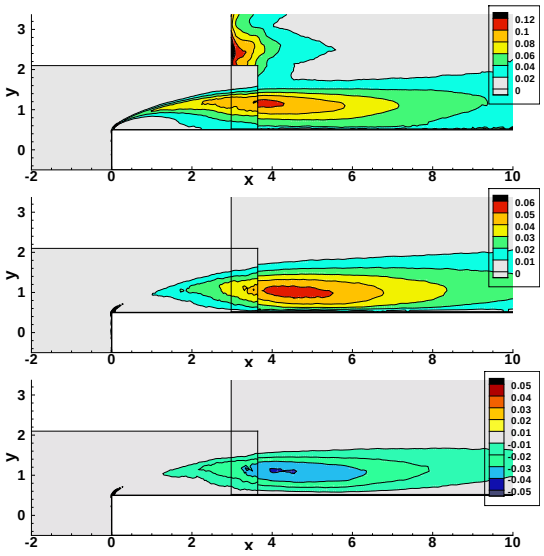

Figure 3. Distribution of Reynolds stresses $\overline{u^2}$ (top), $\overline{v^2}$ (middle) and $\overline{uv}$ (bottom)

The evolution of $C_p^{'} = \sqrt{p'^2}/(\frac{1}{2}\rho.^2 U_o)$ along the x axis is presented in figure 4. A broad maximum of about 0.14 appears a little downstream of the reattachment line $(x/e = 5.5)$. Downstream this line, the $C_{p'}$ decreases sharply to 0.08 at $x/e = 9$. The surface-pressure spectrum at different longitudinal position presented in figure also presents a large band contribution centred at the Strouhal number 0.12. These pressure spectra confirm the decrease of the energy content when x/e is increasing observed on the $Cp^{'}$ evolution. The relative decrease is larger for low frequencies.

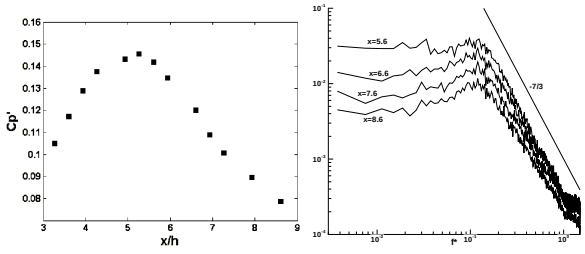

Figure 4. Distribution of $C_p^{'}$ along the longitudinal axis (left), surface-pressure spectrum at different longitudinal positions (right)

Figures 5 shows the power spectrum E_u and E_v of the longitudinal velocity flutuation, u and the vertical velocity fluctuation, v. The power spectra, E_u, is dominated by the low frequencies contribution whereas no clear peak is detected, whatever the vertical position observed. Conversely, E_v, shows a broad but clear peak at the frequency $\frac{fX_r}{U_0} = 0.12$ which is the same as the peak frequency of the surface-pressure spectrum. The disapppearance of this peak in the inner part of the separation bubble ($y/X_r = 0.01$) is in good agreement with the results obtained by Kiya & Sasaki (1983) which suggested that this disappearance may be associated to the contamination of the large scale vortices by smale-scale eddies.

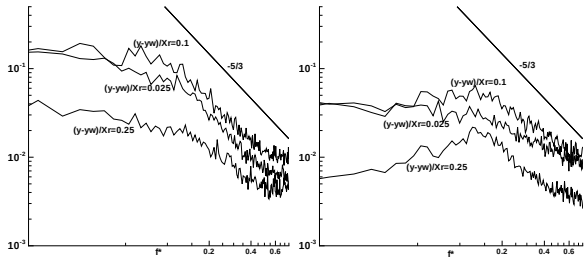

Figure 5. Fluctuating velocity: spectra of u (left) and v (right) at $x/X_r = 1.25$

Figure 6 shows the coherence function of wall pressure (reference point : $x_R = 5.25$), and that of the velocity at $\frac{y-y_w}{X_r} = 0.25$ (reference sensor at $x/Xr = 1$). Both exhibit a very clear peak at the Strouhal number 0.12 along the longitudinal axis. This distribution of the coherence functions corresponds to the signature of the shedding of large-scale vortices from the separation bubble in agreement with the results of previous studies (e. g. Kiya & Sasaki (1983), Cherry *et al.* (1984)). It is also noticeable that pressure-velocity coherence function (not shown here) plotted at a fixed x location versus y presents a similar strong peak, although less pronounced well inside the shear layer, in agreement with the observations made from the velocity spectra.

Estimation of coherent structures

The velocity field correlated with the large scale pressure fluctuations is then educed using the stochastic estimation technique described in the previous section. Figure 7

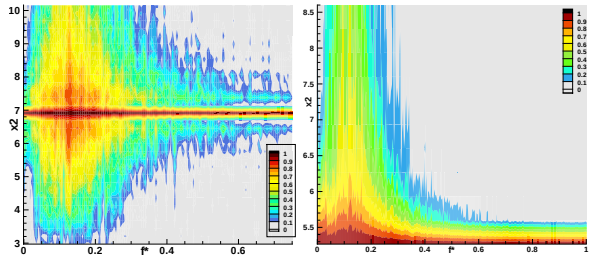

Figure 6. left: Distribution of surface pressure coherence function. ($x_R = 5.25$); right: Coherence function of v on a line $\frac{y-y_w}{X_r} = 0.25$ (reference sensor at $x/Xr = 1$)

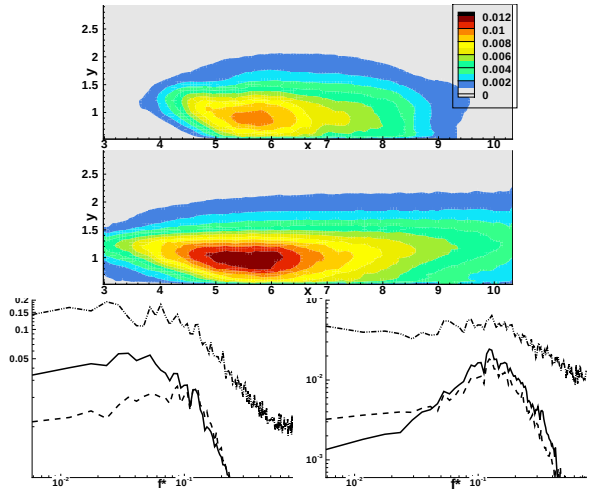

Figure 7. Fluctuating velocity estimated from pressure: top: energy of the fluctuating velocity $\frac{1}{2}(\overline{u^2} + \overline{v^2})$ (top: LSE, bottom: spatio-temporal EPOD approach); bottom: u (left) and v (right) velocity spectra (dashed-dotted line: original velocity, dashed line: LSE, solid line: spatio-temporal EPOD approach) at $x/X_r = 1.25$ and $\frac{y-y_w}{X_r} = 0.1$

(top) presents the 2D fluctuating energy $\frac{1}{2}(\overline{u^2} + \overline{v^2})$ of the estimated field together with that estimated by classical LSE for comparison. The increase of the levels of energy, especially in the regions upstream and downstream of the sensors locations, clearly demonstrates the advantage of the spatio-temporal technique over the LSE, thanks to the convective nature of the flow. Figure 7(bottom) shows velocity spectra of u and v, respectively, for the raw data, the estimated velocity using LSE and the multi-time EPOD, at a point located well inside the shear region. First, in agreement with the previous figure, it is seen that the levels of energy of the estimated is higher using the multi-time EPOD, especially concerning the low frequency content of u. Second, it is clearly seen that while the broad peak at the shedding frequency is hardly visible in the v spectra of the raw data, it is well identified in the spectra of the estimated velocity fields. It is therefore believed that the fluctuating velocity associated with the large scale shed vortices are well separated from the total fluctuating velocity. Although not shown here, spectra of $v - \tilde{v}$, the uncorrelated part of the velocity with the pressure, do not exhibit any broad

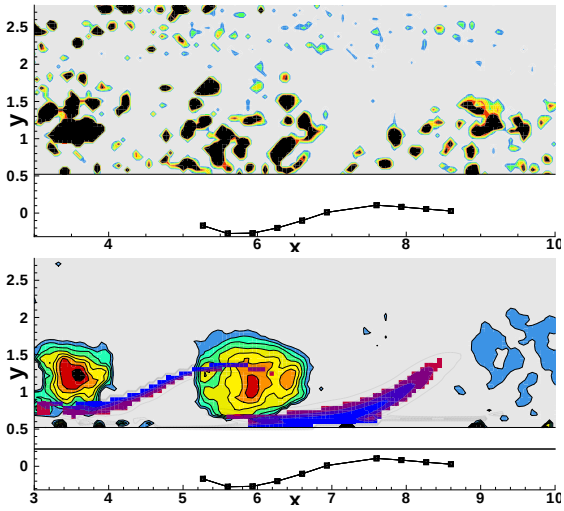

Figure 8. Swirling strengh and FTLE: top: original field, bottom: estimated field from pressure. The measured fluctuating pressure at the same time is represented in arbitrary unit

peak at the shedding frequency. A comment is necessary concerning the relatively low level of energy associated with the estimated large scale structure compared with the total fluctuating energy (see Figure 3). This level of energy (roughly 20% of the total energy) is actually in good agreement with the energy contained in the first modes of a POD performed directly on the velocity fields, showing that the large scale events carry a low part of the total fluctuating energy. Moreover, numerical studies carried out in the same project described in the introduction (e.g. Tran *et al.* (2010)), or at lower Reynolds number (e.g. Lamballais *et al.* (2010)) have clearly shown that the fluctuating velocity is dominated by 3D small scale turbulence.

Figure 8 shows an example of original (top) and estimated (bottom) field taken at the same time. The estimated field clearly exhibits large scale vortices in agreements with previous studies (e.g. Kiya & Sasaki (1985), Lee & Sung (2002)), while they are nearly indistinguishable in the original fields due the fully turbulent nature of the flow. On the same figure are represented the FTLE ridge with the expected topology.

Analysis of large scale vortices evolution after reattachment

Figure 9 shows a sample of the time trace of the location of the vortices (detected from the maximum of swirling strength) and their separating saddle point (detected from the FTLE local maximum). The downstream transport of the vortices appears clearly. The longitudinal evolution of the mean convection velocity U_c deduced from this graph is shown in figure 9 . We see that U_c increases when moving downstream and that the two detection methods give very similar mean values. Note that the increase of U_c is consistant with the longitudinal evolution of the mean velocity field at the center location (discussed below).

Inter-time (dt) statistics between the passage of the vortices at a position x can be deduced. The probability density function of dt is shown in figure 10. This pdf has a strong positive skewness. Further work is presently devoted to this inter-

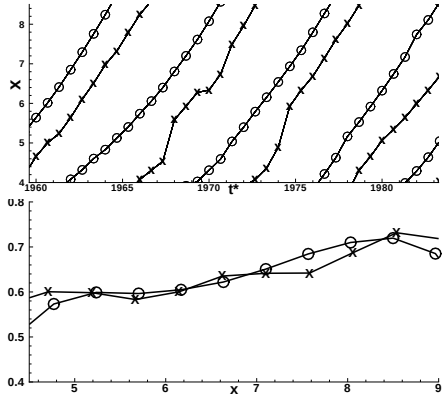

Figure 9. Diagram (t,x) of the detected vortex barycentre and max of FTLE (circle: vortex, cross: FTLE) (top) ; Averaged velocity convection U_c (bottom)

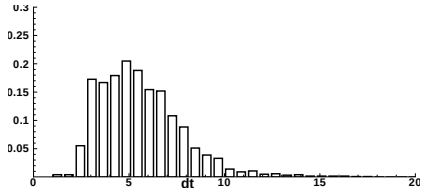

Figure 10. Histogram of the time between two succesive features (swirling strength) at $x = 7$

time sequence. We observe that the global shape of the pdf is of Log-normal type. Bernal (1988) has shown that the amalgamation mechanism in a self-similar shear layer leads to such Log-normal distribution. Our observed distribution may be a consequence of such a distribution in the separated shear layer upstream the reattachement but the interaction with the wall has to be taken into account here. Hoarau *et al.* (2006) have shown that the fluctuating pressure upstream the reattachment is strongly correlated with that dowstream of the reattachmenent. Therefore a simple convection of the vortices emanating from the separated shear layer could lead to such a distribution. Further work is necessary to check this possibility. Note that the mean time interval $\langle dt \rangle = 5.5$ at $x = 7$ is significantly smaller than the period of the velocity signal (T=8) computed from the known Strouhal number ($St = 0.12$). This result may seem contradictory but T is the result of the computation of an eulerian velocity spectrum while $\langle dt \rangle$ takes into account the lagrangian detection of vortices. Model computations, not presented here for brevity, using Lamb Oseen vortices having the measured circulations and locations give the same differences between the two quantities (T and $\langle dt \rangle$).

Figure 11 shows that the mean distance of the vortex center from the wall increases when moving downstream and that their size increases accordingly (size deduced from the area of the structure). Incoherent turbulence generated by vortex/wall interaction is expected to enhance the diffusion of momentum in the structure. Following the same reasoning, we clearly expect the coherence of the structure to decrease when moving downstream. Hoarau *et al.* (2006) have conjectured that these structures, generated in the separated shear layer, loose their kinetic energy in one turn over time scale while being

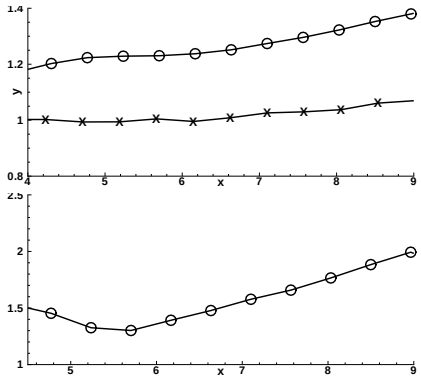

Figure 11. Averaged position y as function of x (top) and averaged surface of vortices (bottom)

Table 1. Characteristic time scales (see text)

Tk	Tk_c	Tc
8.5	6.5	6

transported along the wall in the outer layer. These authors have proposed a simple model equation for the decrease of the coherent kinetic energy based on an equilibrium between advection and dissipation that can be easily solved for constant length scale and transport velocity.

Table 1 shows the average values of the characteristic time scales $Tk = k/(U_c \frac{dk}{dx})$, $Tk_c = k_c/(U_c \frac{dkc}{dx})$ and $T_c = \frac{a}{\sqrt{k_c}}$ between x=6 to 10. Tk_c and T_c are of the same order of magnitude, which means that the rate of decay of coherent kinetic energy scales with the turn over time scale of the educed structures. On the contrary, Tk is much larger than Tk_c. This means that k decays more slowly. It is coherent with the fact that turbulent kinetic energy is generated at the wall and transported by turbulent diffusion in the outer region.

CONCLUDING REMARKS

The aforementioned results showed that the dynamical properties of large scale vortices evolution after reattachment may be evaluated by both Eulerian (swirling strength) and Lagrangian (FTLE) criteria. The results obtained by these two approaches are similar and may be complementary. The irregular character of the shedding process and the presence of intermittent events have been detected from the dispersion of the histogram of the time between two succesive features.

REFERENCES

Adrian, R. J. 1979 Conditional eddies in isotropic turbulence. *Phys. Fluids* **22** (11), 2065–2070.

Bernal, L. P. 1988 The statistics of the organized vortical structure in turbulent mixing layers. *Phys. Fluids* **31** (9), 2533–2543.

Borée, J. 2003 Extended proper orthogonal decomposition: a tool to analyse correlated events in turbulent flows. *Experiments in Fluids* **35**, 188–192.

Cherry, N. J., Hillier, R. & Latour, M. E. M. P. 1984 Unsteady measurements in a separated and reattaching flow. *Journal of Fluid Mechanics* **144**, 13–46.

Garth, C, Li, G. S., Tricoche, X., Hansen, C. D. & H., Hagen 2007 Visualization of coherent structures in transient 2d flows. *Topology Based Methods in Visualization II,Springer, New York* pp. 1–14.

Haller 2001 Distinguished material surfaces and coherent structures in three dimensional fluid flows. *Physica D 149* **149**, 248–278.

Hoarau, C., Borée, J., Laumonier, J. & Gervais, Y. 2006 Analysis of the wall pressure trace downstream of a separated region using extended proper orthogonal decomposition. *Phys. Fluids* **18**, 5.

Kiya, M. & Sasaki, K. 1983 Structure of a turbulent separation bubble. *Journal of Fluid Mechanics* **137**, 83–113.

Kiya, M. & Sasaki, K. 1985 Structure of large-scale vortices and unsteady reverse flow in the reattaching zone of a turbulent separation bubble. *Journal of Fluid Mechanics* **154**, 463–491.

Lamballais, E., Silvestrini, J. & S., Laizet 2010 Direct numerical simulation of flow separation behind a rounded leading edge: Study of curvature effects. *Int. J. Heat and Fluid Flow* **31**, 295–306.

Lee, I. & Sung, H. J. 2002 Multiple-arrayed pressure measurement for investigation of the unsteady flow structure of a reattaching shear layer. *Journal of Fluid Mechanics* **463**, 377.

Perrin, R., Braza, M., Cid, E., Cazin, S., F., Thiele & Boree, J. 2008 Time resolved stereoscopic measurements in the near wake of a circular cylinder at high reynolds number. In *Proc. 14th International symposium on applications of laser techniques to fluid mechanics, Lisbon, July 7-10*.

Ruiz, T., Sicot, C., Brizzi, L. E., Borée, J. & Gervais, Y. 2010 Pressure/velocity coupling induced by a near wall wake. *Experiments in Fluids* pp. 25–+.

Tran, T. T., Perrin, R., Manceau, R. & Boree, J. 2010 Simulation and analysis of the flow over a thick plate at high reynods number. In *ETMM8, Marseille, France*.

Zhou, J., Adrian, R. J., S., Balachandar & Kendall, T. M. 1999 Mechanisms for generating coherent vortex packets of hairpin vortices in channel flow. *Journal of Fluid Mechanics* **387**, 353–396.